Microgravity Science and Technology (2020) 32:761–772
https://doi.org/10.1007/s12217-020-09819-7

ORIGINAL ARTICLE

Design, Simulation and Test of Thermal Control System of Centrifuge for Space Utilization

Yu Zhang [1,2] · Shikui Dong [1] · Ke Wang [2] · Yanlin Zhou [2] · Qiang Sheng [2] · Heping Tan [1]

Received: 27 April 2020 / Accepted: 8 July 2020 / Published online: 16 July 2020

Abstract

Taking centrifuge system for space utilization as the research object, an active air-cooling thermal control system is put forward. Physical models of the centrifuge thermal control system are built on the basis of simplifying assumptions under actual conditions. A numerical calculation model of centrifuge system is established by using the sliding mesh technique and flow resistance model of heat exchanger is introduced based on the porous medium theory. A numerical analysis of the dynamic heat exchange performance of the centrifuge is carried out and the results show the flow and heat exchange characteristics of each part of the system in the dynamic equilibrium state. Also, the centrifuge system and its heat exchange performance test platform are designed and built, and the monitoring probes are placed at the key position. The curves of the whole equilibrium process of key points are obtained and the test condition is consistent with numerical simulation condition. The equilibrium temperatures of the test are in agreement with that of the numerical analysis, which proves that the numerical model and calculation method are accurate. Meanwhile, the test and numerical analysis results can also improve each other to provide data and supporting techniques for in-orbit engineering utilization of manned space station in future.

Keywords Centrifuge system · Space utilization · Air cooling · Semiconductor refrigeration · Performance study

Introduction

As one of the major research directions of space station experiments, space gravity science has emerged the need to do its research in the fields of life science and biotechnology, fluid and combustion etc. Due to the objective existence of gravity on the earth, it is impossible to provide a variable gravity environment beyond the gravitational acceleration. The space environment is an excellent experimental place which can provide a pure variable gravity experimental environment. The simulated variable gravity generated by rotation is the main way to realize space gravity experiment currently. As the main part of the variable gravity science experiment, the task of the thermal control system of the centrifuge system is to control the temperature level of the whole experiment to ensure that it meets the normal working requirements of the test load and other equipment.

With a large diameter of 900 mm, the centrifuge payload is rotated on a fixed axis for a long time. And it causes relative motion between the device loaded on the turntable and the external cooling circulation system. So the thermal control method cannot exist physical connection. Carried out in Express Rack of International Space Station U.S. Density Cabin, the EMCS experiment installed a centrifuge with a diameter of 600 mm, which used the gas-liquid slip ring to dissipate the heat for its payload and controlled the temperature by adjusting the value opening degree to maintain the temperature of the ambient and the incubator between 18 °C to 40 °C (Helleseng et al. 2012; Kamada et al. 2007; Brinckmann 2003). At present, the center rotating shaft position of the centrifuge has been designed and installed with wireless energy transmission device, as the power supply

This article belongs to the Topical Collection: Thirty Years of Microgravity Research - A Topical Collection Dedicated to J. C. Legros Guest Editor: Valentina Shevtsova

✉ Yu Zhang
zhangyu@csu.ac.cn

✉ Shikui Dong
dongsk@hit.edu.cn

[1] School of Energy Science and Engineering, Harbin Institute of Technology, Harbin 150001, People's Republic of China

[2] Key Laboratory of Space Utilization, Technology and Engineering Center for Space Utilization, Chinese Academy of Sciences, Beijing 100094, People's Republic of China

equipment for the entire centrifuge. There is no extra space to install gas-liquid slip ring in the rotating shaft of the centrifuge, so it is impossible to provide cooling source in the form of gas-liquid slip ring. Therefore, all heating equipment of the centrifuge can only dissipate heat through forced convection, namely air cooling. Air cooling system is the key part of the whole thermal control system.

Given that the forced convection is restricted by the air temperature and the refrigeration thermoregulation is insufficiently flexible, it is considered to add the refrigeration module in air-cooling cycle to further reduce the air temperature. The vapor compression refrigeration system is a very mature refrigeration system applied on the ground which can efficiently work within the normal temperature zone based on the sensible heat of working medium. There are three difficulties during the application of this system in space environment:

1. The lubrication and cooling of the compressor in microgravity environment: the normal gravity causes the lubricating oil to flow into the oil groove of the compressor. During the operation of the system, most of the lubricating oil in the oil groove works on the compressor crankshaft and other parts by the oil pump. Meanwhile a small part of the lubricating oil is left in the system, which cannot return to the compressor with the refrigerant. Finally, the amount of oil flowing out is equal to that of flowing into the compressor, so that the whole system can reach the balance. In microgravity, if large amount of oil flows into the cylinder from the oil groove, the compressor will not be lubricated. Thus, it will increase leakage and friction, further which will cause high power consumption and reduce the service life of compressor. At present, several concepts of oil-less vapor compressor under development, including gas bearing, magnetic bearing, self-lubricating material, permanently-sealed (lubrication) bearing and other compressors that do not require lubrication, such as diaphragm compressor, are in the phase of principle prototype research and have no flight experience (Cole et al. 2006; Erickson and Ungar 2013; Grzyll and Cole 2000).
2. The separation between gas and liquid in microgravity environment: in normal gravity environment, the gas-liquid mixture is naturally stratified due to the density difference. While in microgravity, the stratification must be realized by gas-liquid separation technology. The space dynamic gas-liquid separator completes the separation according to the principle of centrifugal force. When the mixture enters the spinning wheel, a large number of droplets are splashed onto the shell of the dynamic gas-liquid separator along with the air flow. Along with the air flow, the droplets accumulate on the shell to a certain amount and then overflow from the air outlet. The existing gas-liquid separation can only achieve the results that no visible droplets in the gas. Still some invisible liquid inflow damage the compressor and it cannot meet the requirement. It can be resolved by means of installing a solenoid valve or check valve to prevent the liquid into the compressor during start-up, or a heating device to vaporize the liquid at the inlet of the compressor in future (Qiu et al. 2015).
3. The evaporator and the condenser are two key parts of the vapor compression refrigeration. The bubble and liquid membrane formed in microgravity cannot leave the wall in time, which will cause the deterioration of the heat exchanger performance (Ma et al. 2014; Zhao and Peng 2011; Zhao 2010; Lv et al. 1997). In summary, there is no mature experience of applying the main components of compression refrigeration system in space microgravity environment, so other thermal control methods are considered in this paper.

Semiconductor refrigeration has the characteristics of simple structure, small size, light weight, short response time and strong controllability, more importantly it is barely affected by microgravity. Given this, a semiconductor refrigeration module is used to refrigerate the air-cooling circuit in the centrifuge system. At present, semiconductor refrigeration chips are mainly used in space probe chip and other occasions with small cooling load, where the hot-end usually applies the fins as the cooling plates to meet the heat dissipation demand, which are barely used in high power refrigeration. The maximum working condition of the centrifuge scientific payload is 600 W for continuous operation, and the heat dissipation capacity allocated to the semiconductor refrigeration module is 200 ~ 300 W. In this case, several refrigerators are required to operate simultaneously (Chakraborty et al. 2006; Zhang et al. 2010; Vian and Astrain 2008; Cheng et al. 2010).

Design of Thermal Control System

Thermal Control Design Strategy

In order to develop a specific thermal control strategy, it is necessary to fully understand the working form and temperature requirements of the main components of the system at first. Due to its performance characteristics of being in rotating working state and continuous high heat consumption, the centrifuge should adopt active air-cooling thermal control system. In view of external thermal control platform can only provide water cooling for the centrifuge, the heat collected by air cooling should be transferred to the external water-cooling system by the gas-liquid heat exchanger to maintain the long-term and efficient operation of the system (Zhang and Tong 2016). Since the life-science payload requires the thermal control system to provide a lower air temperature than the external water cooling, it is obvious that only using water

cooling as the cooling source of the system cannot meet the temperature requirements, so semiconductor refrigeration module should be installed as the key components. Based on the principle of semiconductor refrigeration, the system can obtain cold air below the temperature of external water after secondary cooling by semiconductor refrigeration, to provide a low temperature environment for the life science experiments. This paper focuses on the active thermal control air-cooling system based on semiconductor refrigeration module.

Overview of the System

The schematics diagram and layout of the thermal control system is shown in Fig. 1, which mainly contains semiconductor refrigeration, air-cooling heat exchanger, gas-liquid heat exchanger and fan. The air-cooling circuit adopts the closed self-circulation working mode with no exchange of working medium with the outside. The specific working process is: first driven by the fan, the high-temperature air flows into the gas-liquid heat exchanger to conduct the primary heat exchange with the cooling water and then rises vertically along the air pipe into the air-cooling heat exchanger. Because the cooling side of the semiconductor refrigerator is installed on the surface of the air-cooling heat exchanger, the air will be cooled again when it passes through the inner fins of the heat exchanger. Then the low-temperature air rises vertically to the upper part of the experiment rack along the air supply hose, and flows to the left and right centrifuges and payload modules through the T-pipe. The low-temperature air of the air-cooling circuit fully collects the heat generated from the scientific payload in the rotation test area, and then enters the left and right side return air duct in the lower part, finally converges to the main return air duct and enters the fan to go into the next cycle. The semiconductor refrigeration module for secondary heat exchange is installed between the gas-liquid heat exchanger and the air outlet, which can control the refrigerating capacity according to the actual temperature demand of the system.

Through the liquid-cooling circuit, the external platform provides low-temperature cooling water for the air-cooling system as the cold source of the thermal control system. Due to the limitation of structure layout, it needs to divide the coolant from external through the valve assembly in three parts, one for the gas-liquid heat exchanger and the other two for the hot-end cooling plate of the semiconductor refrigeration module to provide the semiconductor refrigeration with long-term stable thermal path.

Numerical Simulation of Heat Transfer

Because of its complex structure and fixed-axis rotation, the internal flow field of the centrifuge system is complex. It is necessary to predict the centrifuge and internal flow field by means of numerical simulation. Through retaining the main feature of relative motion of centrifuge and air, the effect of object motion on the internal flow can be more accurately

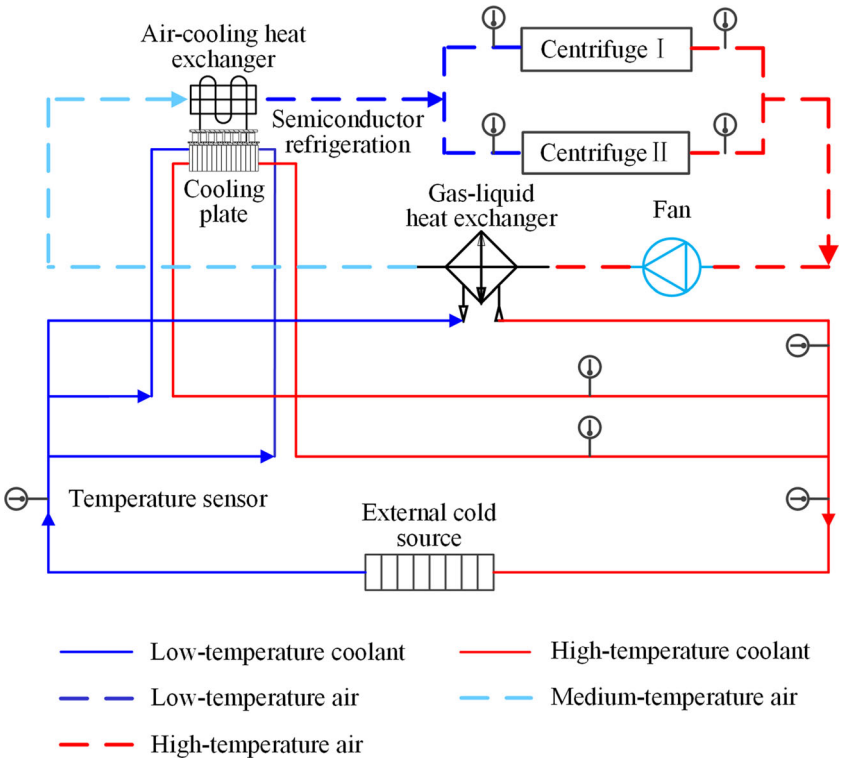

Fig. 1 Schematic diagram of the thermal control system

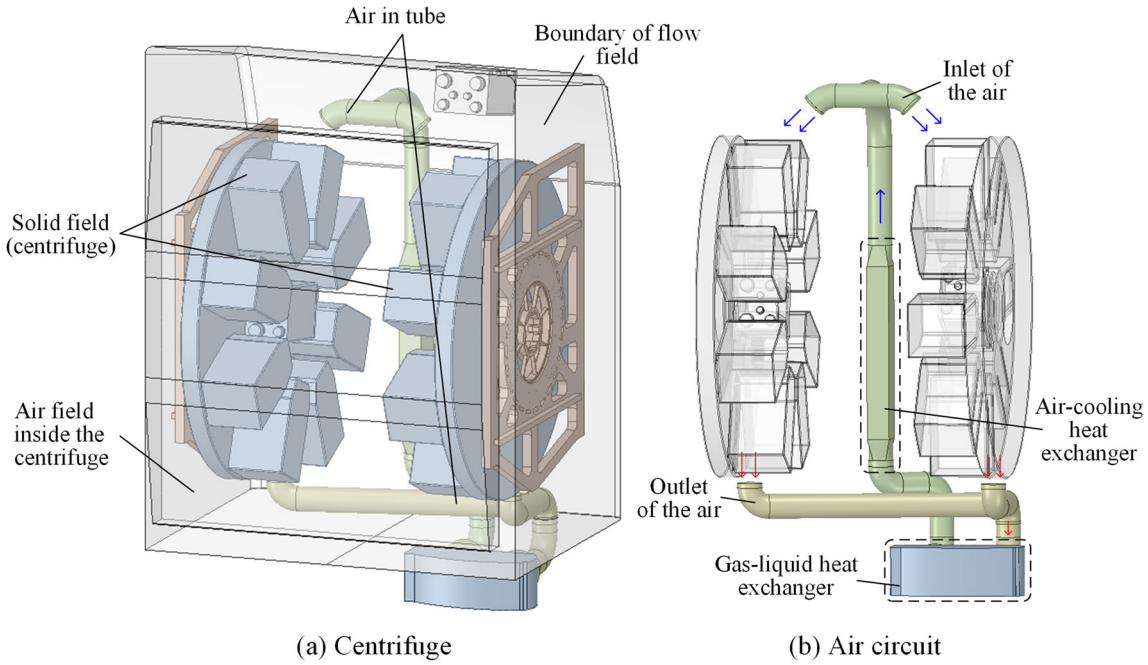

Fig. 2 Three-dimensional physical model of the centrifuge system

simulated. Three-dimensional physical model is established based on reasonable assumptions, as shown in Fig. 2.

Grid Model

The meshes of centrifuge system are generated and polyhedron meshes are adopted. Three layers of prismatic boundary layer grids are added to better simulate the phenomenon that the normal gradient of physical quantity changed rapidly in the velocity and thermal boundary layer, and the thickness of the first layer is 0.0001 m. Y^+ distribution ranges from 40 to 320. The rotating region and the stationary region are meshed respectively, and the meshes of interface of the structure and the fluid region in different regions are divided in the form of common nodes (Xu et al. 2005). The grid model can reflect the details of local geometric features and motion forms. Independence test of grid numbers is carried out and 1.4 million, 2.5 million and 5.6 million grid units are used respectively to calculate the system. The maximum temperature of the centrifuge with three sets of models is obtained. Finally, the result of 2.5 million grids reaches the requirement of grid independence, therefore the grid dimensions of this model is

Fig. 3 Mesh division of the centrifuge system

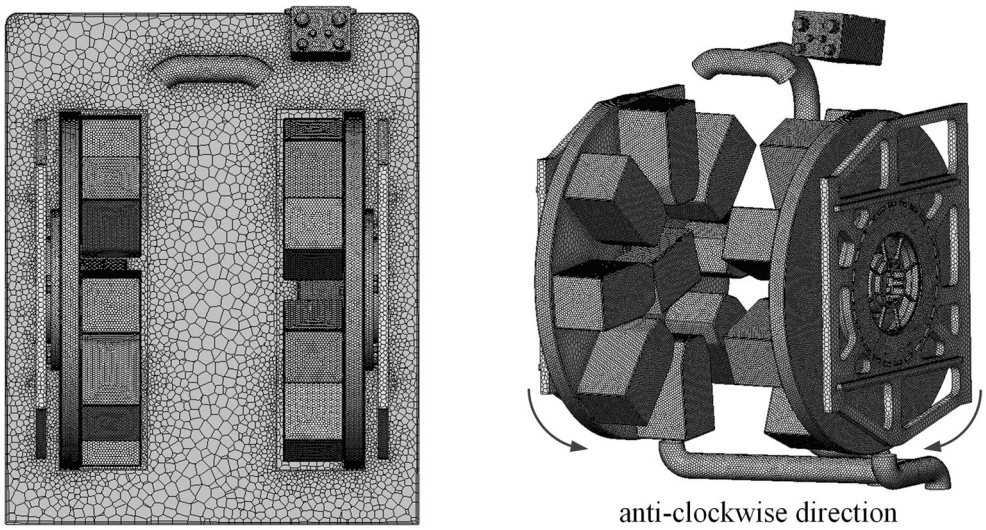

Table 1 Boundary conditions of the full load

Domains	Boundary Type	Unit	Value
Ambient	Temperature	°C	23
Air-Cooling Side	Volume flow rate	cfm	80
	Inlet temperature	°C	17
	Outlet pressure	MPa	0.1(Normal Pressure)
Centrifuge	Rotate speed	rpm	47(anti-clockwise)
	Heat consumption	W	600 W

used to divide the model of the centrifuge system, as shown in Fig. 3.

The structure of the heat exchanger in the model is plate-fin type, and the internal fin structure is complex. If prototype physical modeling is adopted, a lot of computing resources will be consumed. The internal of the heat exchanger is mainly composed of dense fins. The other parts, which are filled with air and connected with each other are divided by fins. These characteristics conform to the porous media. Therefore, the heat exchanger is defined as a porous area, and the influence of fins on the flow and pressure in the heat exchanger is characterized by setting corresponding resistance coefficient on the area (Su et al. 2019; Andriamananjara et al. 2018; Dogonchi et al. 2019).

Boundary Conditions

According to the actual operating conditions in the on-orbit operation control mode of the centrifuge system, the numerical simulation analysis is carried out under the full load condition, and the gravity term is removed. The boundary conditions of the fluid domain and the solid domain in numerical calculation are shown in Table 1, and the physical parameters of the materials involved in the calculation are shown in Table 2.

The test platform for flow resistance measurement of air-cooling heat exchanger and the gas-liquid heat exchanger is built and large amounts of test data about pressure drop at different flow rate are obtained. *P-v* curves are fitted according to these data, as follows:

$$P_{空冷} = 13.72v^2 + 26.44v \tag{1}$$

$$P_{气液} = 6.05v^2 + 6v \tag{2}$$

The commonly used flow rates are selected, and the corresponding relation between pressure drop and flow rate of heat exchanger is shown in Table 3.

Suppose that the air-cooling heat exchanger and the gas-liquid heat exchanger are all homogeneous porous media, the equation is expressed as follows:

$$S_i = -\left(\frac{\mu}{\alpha}\nu_i + C_2\frac{1}{2}\rho|\nu|\nu_i\right) \tag{3}$$

Where S_i (Pa/m) is source item of momentum equation; $\mu$is dynamic viscosity of fluid; $1/\alpha$ ($1/m^2$) is viscous resistance coefficient; v_i (m/s) is velocity in main flow direction; C_2 (1/m) is inertial resistance coefficient; ρ (kg/m^3) is air density.

The momentum source term acting on the fluid creates the pressure gradient in fuild. The formula (3) is converted to obtain the relation between pressure drop and velocity in all directions, as follows:

$$\Delta P = \frac{\mu}{\alpha}{}^{\triangle}n v_i + \frac{1}{2}C_2\rho^{\triangle}n|v|v_i \tag{4}$$

Where ΔP (Pa) is pressure drop in main flow direction; Δn (m) is the length of porous medium in main flow direction.

According to formula (4), the relation between pressure drop and velocity in the flow direction can be also expressed as:

$$\nabla P = a \cdot v^2 + b \cdot v \tag{5}$$

Where, a and b is the coefficient of the fitting quadratic function. According to the coefficient, the viscosity resistance coefficient and the inertial resistance coefficient can be obtained as:

$$\frac{1}{\alpha} = \frac{b}{\mu^{\triangle}n} \tag{6}$$

$$C_2 = \frac{2a}{\rho^{\triangle}n} \tag{7}$$

The values of a and b can be obtained from the *P-v* curves (1) and (2) and then the viscosity resistance coefficient and inertia resistance coefficient of heat exchanger can be calculated, as shown in Table 4.

Table 2 Physical parameters

Name	Material	Density kg/m^3	Heat capacity at constant pressure J/(kg·°C)	Heat coefficient W/(m·K)
Centrifuge	Aluminum alloy	2810	960	130
Fluid	Air	1.165	1005	2.67×10^{-2}
	Aqueous ethylene glycol solution	1041.26	3674	0.455

Table 3 Corresponding relation between pressure drop and flow rate

Volume flow rate ($\times 10^{-3}$ m^3/s)	Velocity (m/s)	Fluid resistance of pipe(Pa)	Pressure drop of air-cooling heat exchanger(Pa)	Pressure drop of gas-liquid heat exchanger(Pa)
9.4	0.88	15	33	10
18.9	1.76	58	89	29
28.3	2.64	127	166	58
37.8	3.52	221	263	96
47.2	4.4	339	382	144
56.7	5.28	483	522	200

Fluid Pressure Field

The pressure distribution of wind field at a certain time after the dynamic equilibrium of the centrifuge system is shown in Figs. 4 and 5. There is an obvious pressure drop process in the air duct along the direction of fluid flow. The pressure at the bottom inlet of the gas-liquid heat exchanger is the highest, and the air-cooling heat exchanger in the ascending section of the air duct is the main pressure-loss component. When the fluid enters the test area from the air inlet pipe, the pressure decreases instantly at the outlet. After the fluid enters a larger space, the pressure distribution is relatively uniform in the whole test area, except that the local pressure of near the upper and lower part of the centrifuge rotating plate increases.

Fluid Velocity Field

Figure 6 shows the distribution of air speed in test area at a certain time. It shows that the maximum velocity in the test area is located in the left and right inlet areas of the top air duct. And the velocity of fluid passing over the upper payload surface of the centrifuge can reach about 10 m/s. Due to the electric control box on the right side of the upper part, the left and right structures are asymmetrical, resulting in a change in the direction of fluid flow and the velocity in the right side is slightly higher than that in the left. After leaving the air duct inlet area, the fluid completely enters the centrifuge rotation area. The space for fluid suddenly becomes larger, and the air speed is greatly reduced. The fluid velocity near the surface of the centrifuge and the payload unit increases, because to some extent the rotation of the centrifuge itself strengthens the

Table 4 Resistance coefficients of heat exchanger

Types of Heat Exchanger	Viscous resistance coefficient $1/\alpha$ ($1/m^2$)	Inertial resistance coefficient C_2 (1/m)
Air-cooling Heat Exchanger	39.1	2.6×10^6
Gas-liquid Heat Exchanger	28.15	1.18×10^5

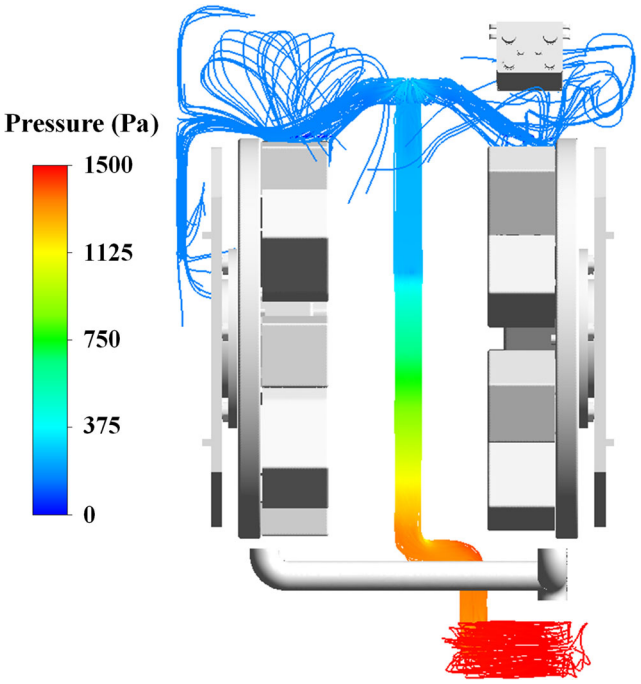

Fig. 4 Pressure streamline of wind field in air pipe

disturbance of the internal fluid and the disturbance also makes the flow direction irregular. The linear velocity along the direction of the centrifuge axis is zero and the disturbance is minimal, resulting in the fluid velocity is the lowest in this direction.

The velocity distribution in air duct is shown in Fig. 7. The air velocity is the lowest in the gas-liquid heat exchanger. After entering the air duct, the air velocity increases rapidly. Then the air reaches the air-cooling heat exchanger, and the

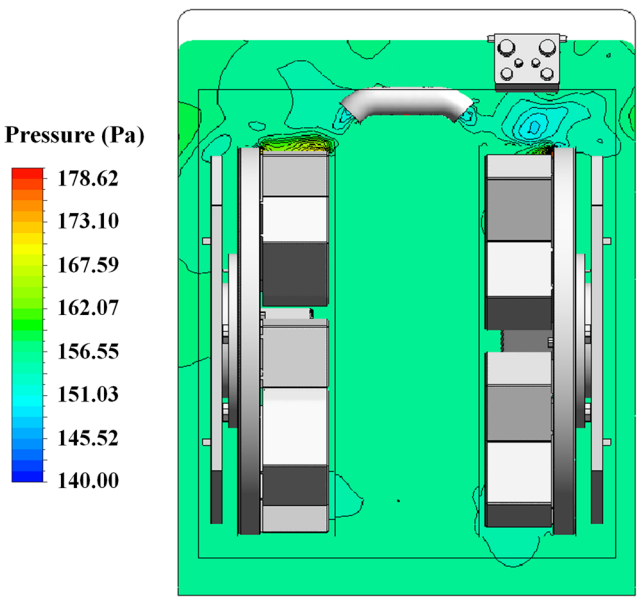

Fig. 5 Pressure contour of wind field in test area

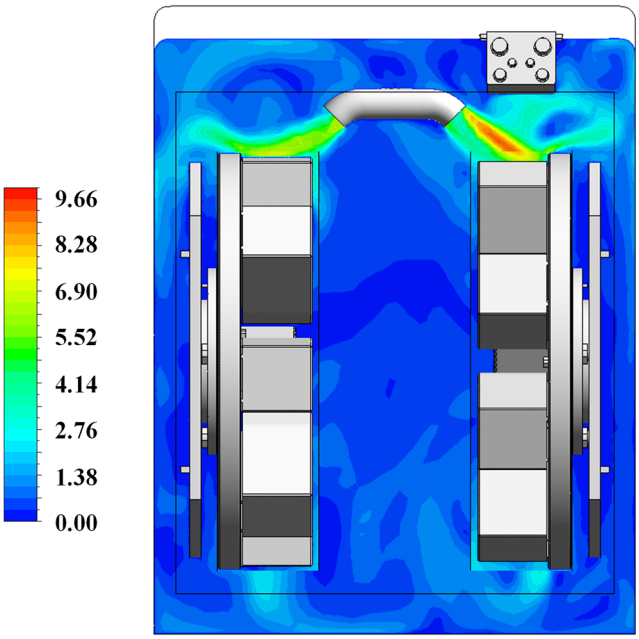

Fig. 6 Velocity contour of wind field in test area

velocity decreases again. Finally, the velocity returns to normal in the upper part of air duct. The reason for the above phenomenons are that the structure of the flow area is complicated due to the fins of the heat exchanger, resulting in the resistance increasing, it makes the velocity of the fluid after entering the two heat exchangers reduce at different degrees. Meanwhile, as the air duct space is small, its internal velocity is generally higher than that in the test area.

The variation curve of heat exchange coefficient on the surface of the payload module with time is shown in Fig. 8,

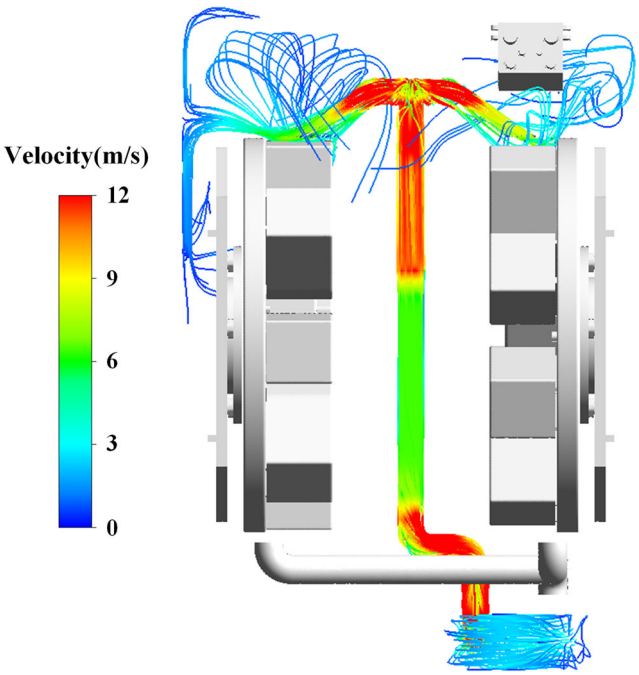

Fig. 7 Velocity streamline of wind field in air pipe

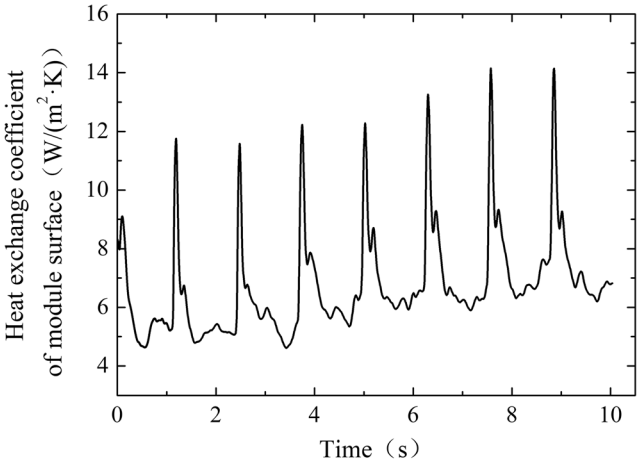

Fig. 8 The variation curve of heat exchange coefficient on the standard module surface

which has obvious periodic oscillation characteristics and whose oscillation period is consistent with the rotation period of the centrifuge. When the module rotates to the air inlet with the centrifuge, the surface air speed is the highest, and the heat exchange coefficient reaches the peak, it becomes the most favorable area for heat exchange. As the module rotates away from the air inlet, the air speed decreases and the heat exchange coefficient drops rapidly. After the module passing the outlet, the air speed increases, and the heat exchange coefficient gradually increases again. And the cycle goes so on.

Fluid-Solid Coupling Temperature Field

The temperature distribution of the system in dynamic equilibrium is shown in Fig. 9. Combined with the above analysis of heat exchange characteristics, it can obtain that due to the increase of heat exchange coefficient on the surface and the heat exchange is enhanced, when the module rotates to the air

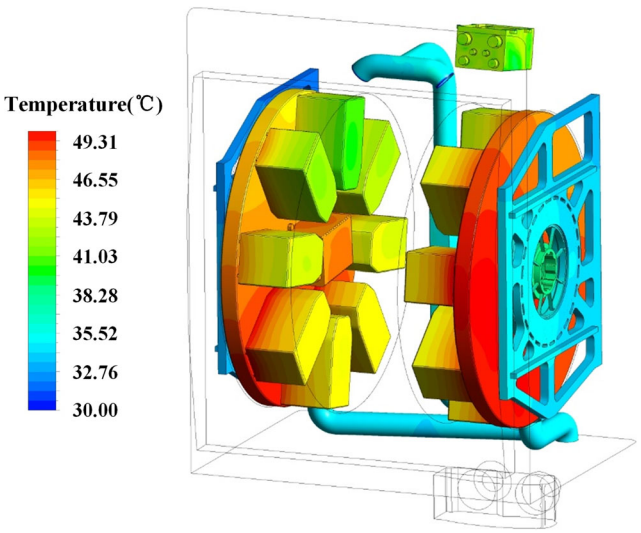

Fig. 9 Three-dimensional temperature distribution of system

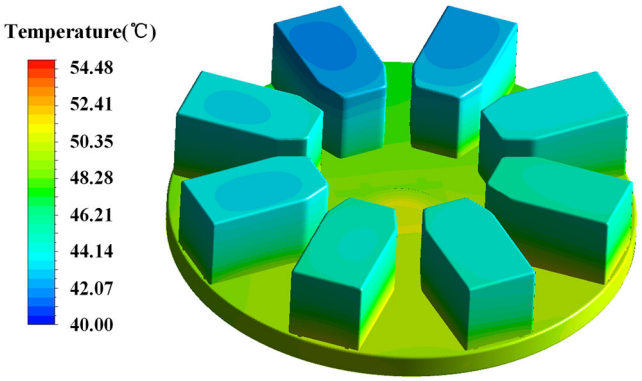

Fig. 10 Three-dimensional temperature distribution of centrifuge rotating plate

inlet, the payload module will have good heat exchange with the low-temperature air. However, because the centrifuge rotates itself, the module quickly switches between the top and bottom area, with only a short stop in the favorable heat exchange area. Due to the existence of its own heat capacity, the module has left the area before the surface temperature significantly decreases. Therefore, large temperature difference will not happen on the same module being in different positions, and the surface temperature reaches 46.5 °C finally. Figure 10 shows the temperature distribution of each payload module. The temperature of the junction between the module and the turntable is high, because the heat consumption of each module is distributed at its bottom.

The temperature distribution of the internal wind field at a certain time is shown in Fig. 11. It indicates that the temperature of the inlet area of the top air duct is about 12 °C. As the air flow rate between the inlet area and the roof of the centrifuge system is high, the disturbance is large, so the heat exchange effect in this area is good, and the temperature only

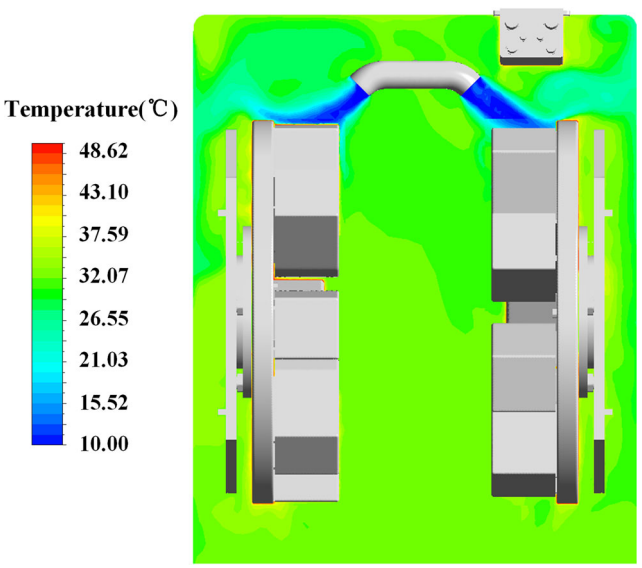

Fig. 11 Temperature contour of wind field in test area

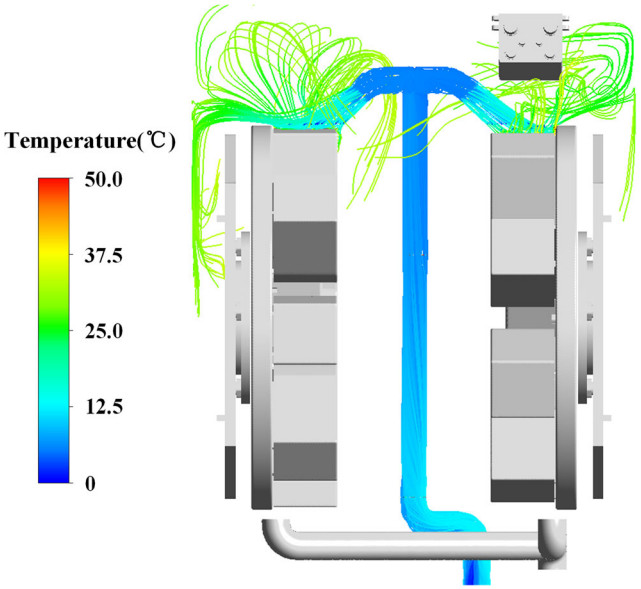

Fig. 12 Temperature streamline of wind field in air pipe

increases to a certain extent. After entering the internal test area, the air fully contacts with the heat dissipation load to make large amount of heat exchange, resulting in a rapid rise in the air temperature. Meanwhile, the upper part installs with low-temperature inlet, so the overall heat exchange effect is slightly better than that of the lower part and its temperature is also slightly lower than that of the lower part. The air temperature around the payload can reach about 32 °C. Figure 12 is the distribution of fluid temperature in the air duct. It indicates that when passing through the air-cooling heat exchanger in the duct, the air is cooled down by the semiconductor refrigeration module, and the air temperature drops significantly. After entering the rotating area, the cold air fully contacts with the heat source, and the temperature rises rapidly.

The dynamic calculation of centrifuge system is realized by numerical simulation, and the distribution of thermal performance parameters in dynamic equilibrium is obtained. But the variation trend of each parameter in the whole process cannot be accurately restored. It is necessary to carry out the heat exchange performance test of the system and monitor the key points of the system with the help of experimental means, and to research the process from the initial state to the later dynamic equilibrium state.

Ground Test

Experiment System

The centrifuge system and its comprehensive performance test platform are built to carry out the thermal performance comprehensive experiment for the system. Parameters such as liquid temperature, liquid flow rate, liquid pressure, temperature

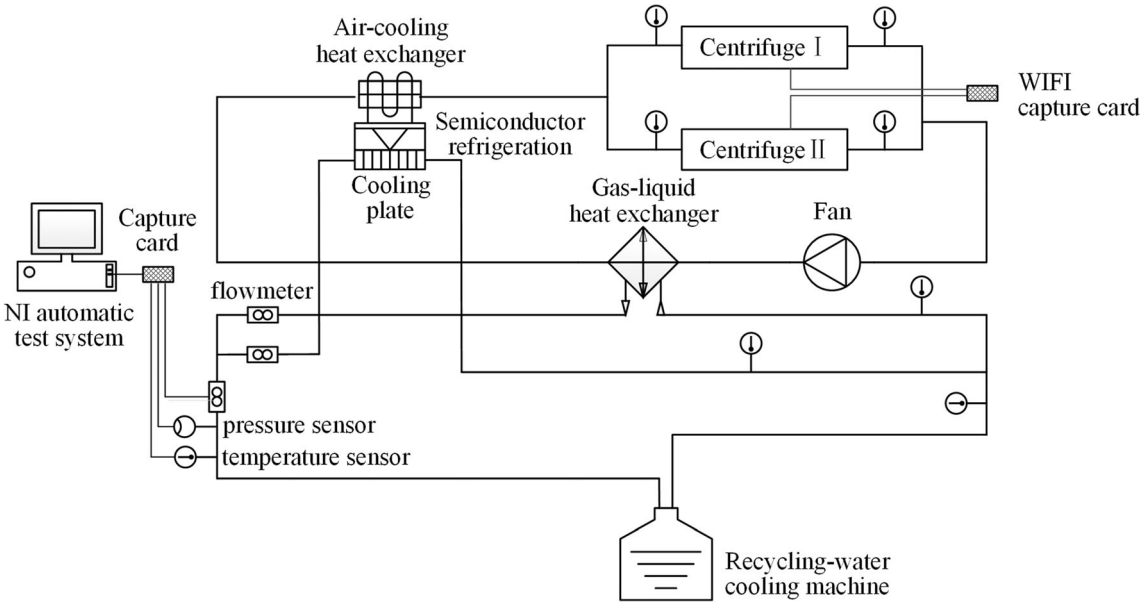

Fig. 13 Schematic diagram of the thermal performance test platform

and velocity of gas are collected to obtain heat exchange performance and flow resistance performance of the system. Figures 13 and 14 are the diagram and photo of the comprehensive thermal performance test platform of the centrifuge thermal control system. The test platform is mainly composed of centrifuge system, semiconductor refrigerator, air-cooling heat exchanger, gas-liquid heat exchanger, liquid-cooling cold plate, fan, recycling-water cooling machine, data collection card and NI automatic test system. The recycling-water cooling machine is composed of pump, compressor, evaporator, condenser and expanding value, which drives the liquid-cooling circuit and also provides the cold source for the whole experimental system. The fan provides the driving force for the air-cooling circuit. The heat exchanger is the link between the air and the liquid and its function is to transfer the heat from the air to the coolant. The data test and collection system are composed of NI automatic test system, WIFI capture card, temperature sensor, pressure sensor and flow sensor. During the experiment, the electric heater is used to simulate payload to continuously release heat and supplied by a stabilized DC power, which adjusts the supply voltage to realize different working conditions.

Fig. 14 Pictures of the thermal performance test platform

Experiment Conditions

The experiment conditions are set according to the operating conditions. The operating parameters under full load startup work condition are shown in Table 5, basically consistent with those of the numerical simulation conditions. The result of them can verify with each other.

Table 5 Experiment parameters of the full load

Parameter	Value
Heat Rate of centrifuge I (W):	280
Heat Rate of centrifuge II (W):	290
Speed of centrifuge I (rpm)	49(clockwise)
Speed of centrifuge II (rpm)	43(clockwise)
Temperature of circulating-water machine (°C):	25.2
Ambient temperature (°C)	23
Flow rate of Cold plate1 (L/h)	29.40
Flow rate of Cold plate 2 (L/h)	30.26
Flow rate 3(L/h)	60.53

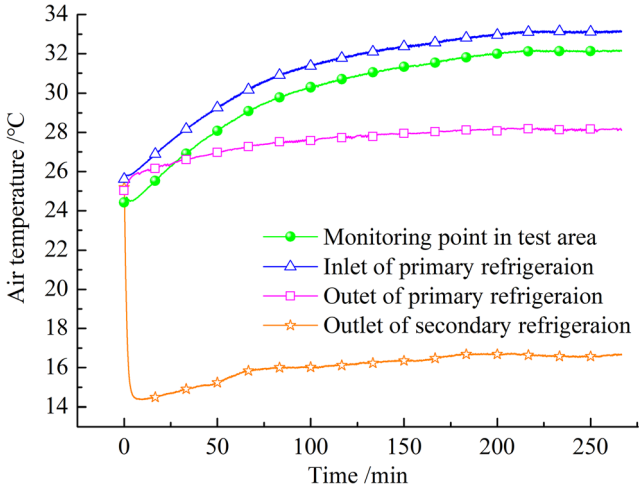

Fig. 15 Temperature variation curves of air in air-cooling circuit

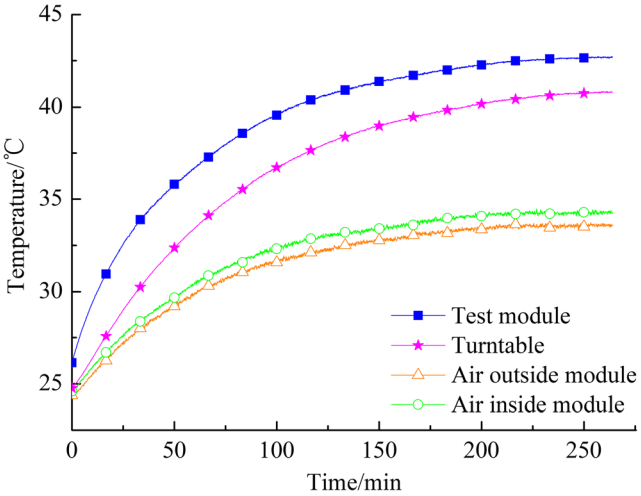

Fig. 17 Temperature variation curves of the payload module and the ambient

Result Analyses

Figure 15 shows the temperature of each key point in the internal air-cooling circuit of the centrifuge with time. After reaching to the full load condition, the payload continues to dissipate heat. The air temperature monitoring point is set in the test area and the temperature of the point gradually increases with time. After 220 min, the temperature reaches balance and the equilibrium temperature is 31 °C. Meanwhile the air temperature around the payload is about 32 °C in numerical simulation calculate result, which is in agreement with the test data above.

In this process, the change rate of air temperature with time is large in the early period and low in the later period. The heat exchange environment at the primary refrigeration inlet is basically consistent with the monitoring point in test area, so the air temperature change trend is roughly the same as that at the monitoring point in test area. However, there is further heat exchange between the air and all the payloads, the temperature of primary refrigeration inlet is higher than that at the monitoring point in test area at each moment. After passing through the air side of the gas-liquid heat exchanger, the air reaches the primary cooling outlet, where heat exchange occurs between the air and the refrigerant of the liquid side at all times, so the temperature changes very slowly after starting full load. The secondary refrigeration outlet is the inlet of the test area. The air temperature rapidly drops from environment temperature to lower temperature within 5 min after starting TEC refrigeration module, and then the temperature rebounds slightly until the temperature reaches balance at the point around 180 min, and finally remains constant at 16.6 °C. The reason for the temperature inflection point is that at the beginning of the centrifuge system startup, the air temperature drops rapidly under the drive of the refrigeration module. At that time, the refrigeration module is the leading factor. In the later period, with the sufficient heat exchange between the payload module

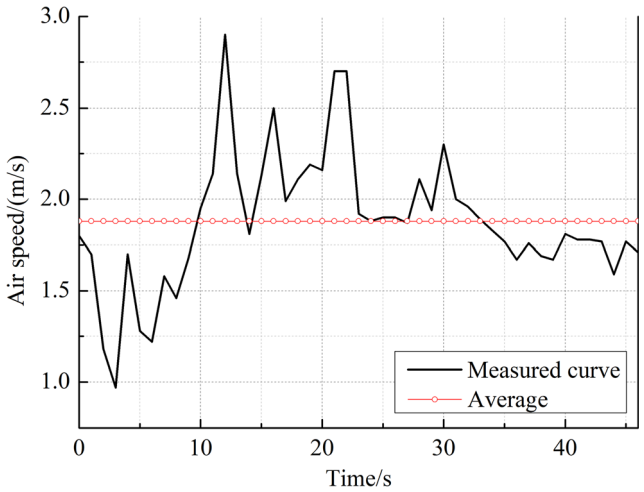

Fig. 16 Air speed curve of inlet in test area

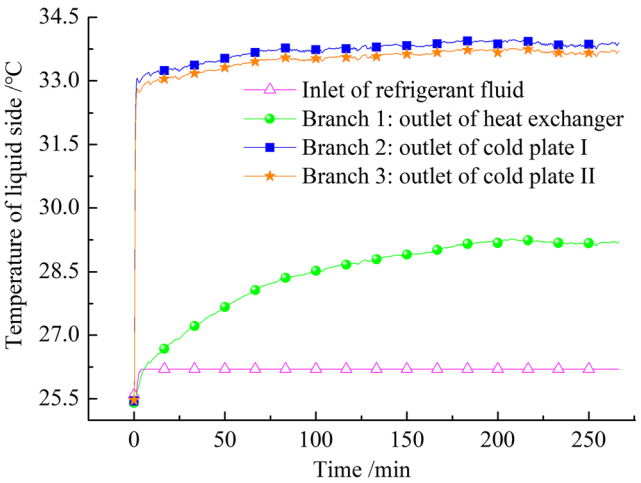

Fig. 18 Temperature variation curves of refrigerant

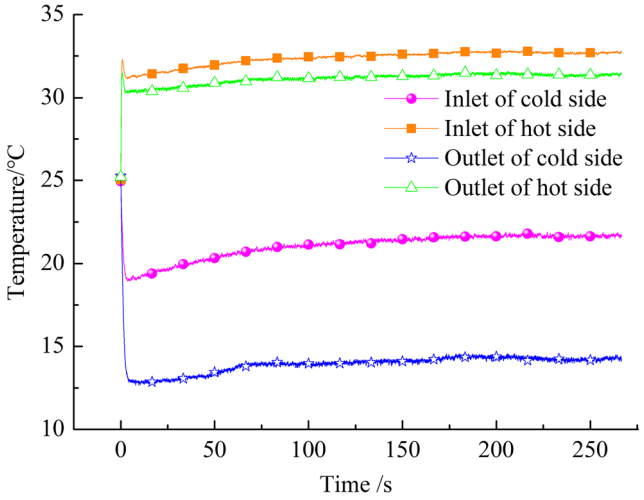

Fig. 19 Temperature variation curves of semiconductor refrigeration

and the air, the overall temperature of the system increases, and the temperature of the secondary refrigeration outlet rises slightly. The air speed of the secondary refrigeration outlet, namely the inlet of the test area, exists disturbance to some extent, with an average value about 2 m/s, as displayed in Fig. 16.

The temperature variation of the payload module and the ambient with time is shown in Fig. 17. Due to the continuous heat dissipation of the test module, its temperature gradually increases with time. The temperature reaches balance after 230 min, the final temperature maintains at 42.7 °C. The numerical simulation result reveals that the surface temperature of the payload module is 46.5 °C. Calculation error is 8.9%, which proves that the numerical model is accurate. The turntable is used as the installation surface of the test module and also one of the heat dissipation ways of the payload module. But, due to the structure of the turntable, the contact area is small, so there is an obvious temperature difference between the scientific test module and the turntable. The convective heat transfer of air is another heat dissipation way of the module. By the rotating speed of the turntable, it can be obtained that the linear velocity on the outside of the module is 4.4 m/s. Herein, the heat exchange coefficient is low, and the effect on payload module of air heat dissipation is lower than that of the turntable heat conduction. The inside speed of the module is slightly lower than that of the outside, so the inside temperature is slightly higher than that of the outside.

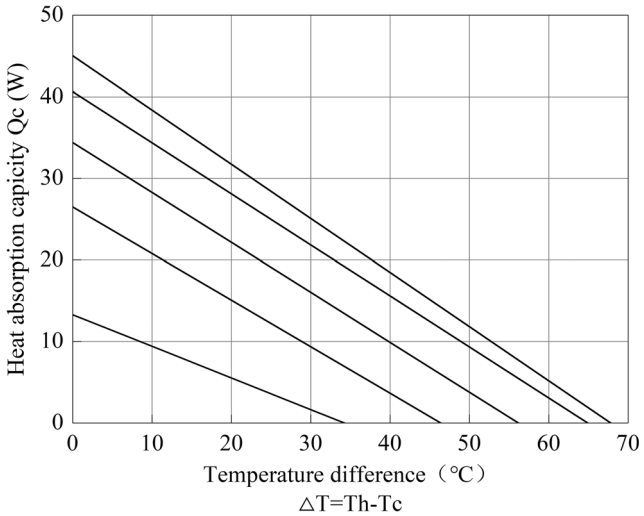

Fig. 20 Performance curves of semiconductor refrigeration

Figure 18 reveals that the temperature variation of refrigerant with time. The total inlet temperature of the liquid-cooling circuit is 26.4 °C, which is divided into three branches by the flow distribution valve. The liquid temperature of the outlet branch of the gas-liquid heat exchanger is 29 °C, and the heat exchange capacity at the liquid side is 194 W. Combined with the temperature of the inlet and outlet of the gas-liquid heat exchanger at the gas side are respectively 33 °C and 28 °C, as displayed in Fig. 15. According to formula of heat exchanger efficiency $\eta = (\Delta T)_{W\min side}/T_{1in} - T_{2in}$, it obtains that the efficiency of gas-liquid heat exchanger is 74.6%.

The composition of the other two branches is basically the same, and the outlet temperature of the cooling plates are respectively 33.9 °C and 33.7 °C, and the corresponding heat exchange capacity are 245 W and 239 W, which are the heat released from the hot-end of semiconductor refrigeration module. Combined with the power supply of the refrigeration module, on the premise of ignoring heat leakage, the overall refrigeration coefficient can be calculated as 0.7.

Under the action of semiconductor refrigerator, the hot side temperature of its two installed sides rises sharply, while the cold side temperature drops rapidly. After the temperature reaches the balance, the corresponding installation temperature is different due to the different temperature of fluids from the cold and hot side of the refrigerators at different positions, resulting in different working point of each refrigerator. Taking the inlet and outlet of air-cooling heat exchanger as an example, the temperature difference at the inlet is 11 °C, and that at the outlet is 17 °C, as shown in Figs. 19 and 20 provides the heat absorption capicity variation with temperature difference of semiconductor refrigeration and it can be obtained that the refrigerating capacity of the inlet and outlet refrigerator is 12 W and 15 W respectively.

Conclusions

Based on environmental requirement of space operation, a thermal control system mainly focused on the centrifuge system operating in microgravity environment is put forward. On the reasonable assumptions, a thermal control system model

of the centrifuge is established. The performance and influence factors of heat exchange is obtained under the dynamic equilibrium in microgravity environment by numerical simulation. Also, the performance test platform is built to test the whole heat balance process, and the conclusion as follows:

1. The centrifuge system for space utilization applies the active air-cooling system, and it can control the semiconductor refrigeration module to realize different refrigerating capacity according to the actual temperature requirement.
2. Results of numerical simulation show that: under dynamic equilibrium in microgravity environment, the outlet temperature of the air duct is 12 °C with the refrigeration module working and the air speed is 10 m/s. When the air temperature of test area is 32 °C and the payload module reaches 46.5 °C in the equilibrium. The results meet the requirement of scientific payload.
3. The heat exchange coefficient of the payload module surface changes periodically with the rotation of the centrifuge, whose variation period is equal to the rotation period and when the module rotates to the air inlet, the coefficient reaches the maximum. The payload module itself has no periodic temperature change due to its heat capacity.
4. The data of the equilibrium process is obtained by the test. The equilibrium time of the internal wind field and the payload module is about 4 h, and the equilibrium temperature is 31 °C and 42.7 °C. Meanwhile the data is basically consistent with the numerical simulation results, which proved that the gravity has little influence on the heat exchange performance. And the data of the ground test can support the heat exchange performance research of the centrifuge thermal control system under microgravity condition.

Acknowledgments The work presented is sponsored by the Manned Space National Science and Technology Major Project, which is gratefully acknowledged.

References

Andriamananjara, K., Moulin, N., Bruchon, J., Liotier, P.J., Drapier, S.: Numerical modeling of local capillary effects in porous media as a pressure discontinuity acting on the interface of a transient bi-fluid flow. Int. J. Mater. Form. **12**, 675–691 (2018). https://doi.org/10.1007/s12289-018-1442-3

Brinckmann, E.: New facilities and instruments for developmental biology research in space. Adv. Space Biol. Med. **9**, 253–280 (2003). https://doi.org/10.1016/S1569-2574(03)09010-5

Chakraborty, A., Saha, B.B., Koyama, S., Ng, K.C.: Thermodynamic modelling of a solid state thermoelectric cooling device: temperature-entropy analysis. Int. J. Heat Mass Transf. **49**, 3547–3554 (2006)

Cheng, C.H., Huang, S.Y., Cheng, T.C.: A three-dimensional theoretical model for predicting transient thermal behavior of thermoelectric coolers. International Joumal of Heat and Mass Transfer. **53**, 2001–2011 (2010)

Cole, G.S., Scaringe, R.P., Grzyll L.R., Ewert, M.K.. Development of a Gravity-Insensitive Heat Pump for Lunar Applications. https://ntrs.nasa.gov/search.jsp?R=20060056224. Published 01 January (2006)

Dogonchi, A.S., Waqas, M., Seyyedi, S.M., Hashemi-Tilehnoee, M., Ganji, D.D.: Numerical simulation for thermal radiation and porous medium characteristics in flow of CuO-H_2O nanofluid. Journal of the Brazilian Society of Mechanical Sciences and Engineering. **41**, 249 (2019). https://doi.org/10.1007/s40430-019-1752-5

Erickson, L.R., Ungar, E.K.. Vapor compression and thermoelectric heat pumps for a Cascade distillation subsystem: design and experiment. AIAA SPACE Forum (2013). https://doi.org/10.2514/6.2013-5397

Grzyll, L.R., Cole, G.S.. A prototype oil-less compressor for the international space station refrigerated centrifuge. International Compressor Engineering Conference. 121–128 (2000)

Helleseng, K.O., Grønnevik, A., Fossum, K.R., Kittang, A.I., Iversen, T.H.. Utilization of the european modular cultivation system-opportunities and support functions. International Astronautical Congress (2012). https://doi.org/10.2514/6.IAC-05-A2.5.01

Kamada, M., Omori, K., Nishitani, K., Hoson, T., Shimazu, T., Ishioka, N.: JAXA space plant research on the ISS with European modular cultivation system. Biological Sciences in Space. **21**(3), 62–66 (2007). https://doi.org/10.2187/bss.21.62

Lv, C.D., Wang, H.Q., Li, F.J., Cheng, S.M.: The feasibility of simulation testing under Normal gravity of two-phase flow boiling heat transfer under microgravity. J. Huazhong Univ. of Sci. & Tech. **25**(7), 103–105 (1997)

Ma, R., Wu, Y.T., Liu, G., Ma, Z.F.: Calculation of vapor compression heat pump evaporator gravity-independent. CIESC Journal. **65**(S1), 125–129 (2014)

Qiu, R.H., Wu, Z.Q., Gao, F., Shang, W.J., Huang, Y.H.: Experimental study on performance of a space dynamic gas /liquid separator aboard zero-g plane. Manned Spaceflight. **21**(3), 212–216 (2015)

Su, J.W., Chai, G.L., Wang, L., Cao, W.D., Yu, J.B., Gu, Z.L., Chen, C.G.: Direct numerical simulation of pore scale particle-water-oil transport in porous media. J. Pet. Sci. Eng. **180**, 159–175 (2019). https://doi.org/10.1016/j.petrol.2019.04.078

Vian, J.G., Astrain, D.: Development of a heat exchanger for the cold side of a thermoelectric module[J]. Appl. Therm. Eng. **28**, 1514–1521 (2008)

Xu, Z.H., Wu, Y.L., Chen, N.X., Liu, Y., Zhang, L., Wu, Y.Z.: Simulation of turbulent flow in pump based on sliding mesh and RNG k-ε model. J. Eng. Thermophys. **26**(1), 66–68 (2005)

Zhang, Y., Tong, T.F.: Thermal control scheme study of scientific experiment rack of new manned space station. Procedia Engineering. **157**, 374–381 (2016). https://doi.org/10.1016/j.proeng.2016.08.379

Zhang, H.Y., Mui, Y.C., Tarin, M.: Analysis of thermoelectric cooler performance for high power electronic packages. Appl. Therm. Eng. **30**, 561–568 (2010)

Zhao, J.F.: Two-phase flow and pool boiling heat transfer in microgravity. Advances in Mechanics. **40**(4), 460–470 (2010)

Zhao, J.F., Peng, H.: Review on in-tube condensation in different gravity conditions. Advances in Mechanics. **41**(6), 702–710 (2011)